

Article

# Microstructural and Corrosion Behavior of High Velocity Arc Sprayed FeCrAl/Al Composite Coating on Q235 Steel Substrate

Ndumia Joseph Ndiithi <sup>1</sup>, Min Kang <sup>1,\*</sup>, Jiping Zhu <sup>2</sup>, Jinran Lin <sup>1</sup>, Samuel Mbugua Nyambura <sup>1</sup>, Yuntong Liu <sup>1</sup> and Fang Huang <sup>1</sup>

<sup>1</sup> College of Engineering, Nanjing Agricultural University, Nanjing 210031, China

<sup>2</sup> Ministry of Agriculture and Rural Affairs, Nanjing Research Institute for Agricultural Mechanization, Nanjing 210000, China

\* Correspondence: kangmin@njau.edu.cn; Tel.: +25-58606578

Received: 15 July 2019; Accepted: 21 August 2019; Published: 24 August 2019



**Abstract:** High velocity arc spraying was used to prepare FeCrAl/Al composite coating on Q235 steel substrate by simultaneously spraying FeCrAl wire as the anode and Al wire as the cathode. The composite coating was sprayed with varying voltage and current to obtain optimum coating characteristics. FeCrAl coating was also prepared for comparison purposes. The surface microstructure of the coatings was characterized by scanning electron microscope (SEM) and X-ray diffraction (XRD). The average microhardness of the coatings and the substrate was analyzed and compared. Corrosion resistance was investigated by means of electrochemical tests. The image results showed that a lamellar structure consisted of interwoven layers of FeCrAl and Al. Al and FeCr constituted the main phases with traces of oxides and AlFe intermetallic compounds. The average porosity was reduced and microhardness of the coatings was improved with increasing voltage and current. The FeCrAl/Al coating formed alternating layers of hard and ductile phases; the corrosion resistance of the coatings in the sodium chloride (NaCl) solution depended on the increase in Al content and spray parameters. The corrosion resistance tests indicated that FeCrAl/Al coating had a better corrosion resistance than the FeCrAl coating. FeCrAl/Al can be used to coat steel substrates and increase their corrosion resistance.

**Keywords:** high velocity arc spraying (HVAS); FeCrAl/Al composite coating; polarization tests; surface morphology

## 1. Introduction

Steel components are used extensively in the chemical, bridge construction, agricultural equipment, and other industries. Q235 steel is a widely used material in these industries for its relatively good mechanical properties. Q235 steel is a common material for the main components of mechanical equipment. Besides having relatively lower cost than stainless steels and superalloys, this material has good machinability and welding performance [1]. Due to the complex working conditions where friction, high temperature, and corrosion occur frequently, the durability and service life of the steel is reduced. Thermally sprayed coating methods can be used to increase service life of these machine parts and structures made of Q235 steel. It is therefore of great value and significance to study the structure and properties of coatings on Q235 steel.

Among different thermal spray processes used to protect steel surfaces, arc spraying method is widely used for anticorrosion coatings [2]. The high velocity arc spraying (HVAS) is an important technique used to protect steel surfaces and small metal components from corrosion. The material to

be coated is introduced in the arc in form of two consumable electrodes. In the process, two similar or dissimilar wires are used to form an arc at the tip of the spray gun the arc melts the wires and the high compressed air is blown directly behind the point of contact, atomizing and projecting the melted particles onto the surface [3,4]. HVAS is an improved design of the electric arc wire spray because of its high velocity and better atomizing of melted droplets. According to Gedzevicius et al., arc sprayed coatings offer dense structure coatings with high bond strength and have several benefits such as low running cost, high deposition rate of metallic coatings, and high efficiency [5,6]. The sprayed coating layer acts as a corrosion barrier as well as provide cathodic protection for the substrate against corrosive environment. Thermally sprayed coatings not only provide resistance to corrosion but also against high and alternating temperatures and abrasion/erosion resistance [7]. However, arc spraying method forms oxides in coatings due to the presence of oxidation of the molten material by air, which reduces quality of coatings [8].

HVAS can be used to prepare composite and alloy coatings by an alternative method of arc spraying two dissimilar metal wires or cored wires to form pseudo-alloys. Spraying of different metal wires offers a variety of possibilities in producing composite coatings. The resulting coatings combine the properties of both materials to achieve better properties than individual materials [9]. However, it has been noted that using two different metal wires to form composite coatings by arc spraying can be challenging due to the difficulty in the electrode control. The combination of two different wires leads to arc instability because of the unbalanced melting rates of the metals at the electrode tips. In this case, however, the higher melting point materials can be used as the anode, while the lower melting point materials used as the cathode in order to obtain a better droplet dispersion produced from the corresponding wires [10]. Some of the composite coatings formed by arc spraying include but not limited to nickel–aluminium intermetallic compound coatings, zinc–aluminium alloy, 321 stainless steel–aluminum wires, and FeCrAl–aluminum–bronze [11,12].

In arc spraying process a coating is formed when molten droplets solidify on impact; the coating is built up by continuous layers of the splats that stack on top of each other [13,14]. The internal phase composition of the coatings mostly contains pores, oxides, and semi-melted particles, which are dependent on the spray parameters that are used. Both the particle velocity and the temperature of the sprayed particles at the impact have a strong influence on the flattening ratio and the contact of the particle, which in turn influence the solidification rate, adhesion and ultimately the microstructure. The excessive particle temperature would cause substrate damage and result in low bonding strength [15]. The amount and distribution of these defects, as well as other coating properties as for instance thickness, hardness and bond strength, will be defined by the selected spray parameters. Therefore, the correct choice of the spray process as well as respective parameters such as arc current, arc voltage, particle velocity, and spray distance are very important for the deposition.

FeAl intermetallic coatings have been widely used in the recent years due to their low density, availability of the raw materials, and good sulfidation resistance properties and wear resistance. The iron aluminide coatings have outstanding high temperature abrasive and erosion properties. These FeAl intermetallic properties can be modified by adding third components [13,16,17]. Aluminum has good properties such as high strength-to-weight ratio and good corrosion resistance. High temperature corrosion resistance of FeCrAl can be improved by spraying Aluminium coating on the FeCrAl coating. High Cr content in Fe alloys improves the high temperature oxidation and corrosion resistance as well [18]. Corrosion studies on Aluminum and Stainless steel have been extensively studied in various environments. Much of the knowledge attributed the corrosion resistance of Al due to its protective film of  $\text{Al}_2\text{O}_3$  and stainless steel due to the passivating layer of  $\text{Cr}_2\text{O}_3$ . Moreover, a recent study on corrosion behavior of Zinc and Zn–Co alloy electrodeposits Zn–0.89 wt.% Co exhibited higher corrosion resistance due to its smaller grain size than the coating with coarser grain size. The higher grain boundary density in the coating with smaller grain size sped up formation of a stable and protective film. Zinc alloy coatings display sacrificial cathodic protection as is the case in corrosion behavior of zinc-rich epoxy

primers. The reduction of the coating porosity lead to enhancement of the coating physical barrier as well as enhanced zinc sacrificial cathodic protection [19,20].

The purpose of this study is to improve the corrosion properties of high velocity arc sprayed FeCrAl coatings by simultaneously arc spraying FeCrAl and Aluminum wires. The emphasis is to combine the individual properties of the two materials. FeCrAl coating was sprayed alone for comparison purposes. The surface morphology tests, microhardness of the coatings and substrate were examined in this research. Corrosion behavior of the FeCrAl/Al coating was studied using potentiodynamic polarization tests.

## 2. Materials and Methods

### 2.1. Substrate and Feedstock Material

The substrate material was Q235 steel plate of dimensions 50 mm × 30 mm × 8 mm. Shaping of the substrate was done to avoid the sharp edges and improve adherence of the coating to the substrate [4]. Before coating process, the steel substrate surfaces were grit blasted using compressed air and abrasive grit blasting that was carried out in a hand operated cabinet type blast cleaning machine. The substrate was blasted with 18-mesh steel grit at a pressure of 0.6 MPa. Grit blasting was done to improve the mechanical bonding, surface activation and cleaning rust and oxide scale. After grit blasting, the specimen was blow dried by compressed air to remove any debris on the surface and a surface finish controlled to surface roughness,  $R_a$  of about 4  $\mu\text{m}$  was achieved.

The spraying feedstocks were commercially available FeCrAl and aluminium wires, both 2 mm in diameter. The chemical compositions of the spraying wires, as provided by the vendor, are listed in Table 1. According to a previous experiment, it is proven that material with higher melting point is used as anode and material with lower melting point as the cathode. This can improve the arc stability owing to the relatively unbalanced melting rates at the two electrodes [11]. Owing to the higher melting point, FeCrAl wire was used as the anode and Aluminium wire as the cathode. The dual FeCrAl wires was used to prepare the FeCrAl coating for comparison purposes.

**Table 1.** Chemical composition of the spraying wires FeCrAl and Al (wt.%).

Feedstock Wire	Al	Cr	Fe
FeCrAl	6	26	Balance
Al	99.9	–	–

### 2.2. Spraying Process

In the arc spraying process, an electric arc is struck between the two consumable electrodes to form molten droplets. The molten droplets were atomized by the compressed air onto the Q235 Steel substrate. The arc spraying process was conducted with the LSARC arc spraying machine equipment, as shown in Figure 1 below (Shanghai Liangshi Co., Ltd., Shanghai, China), at a standoff distance of 200 mm, a primary air pressure of 0.65 MPa, and a secondary air pressure of 0.55 MPa. The FeCrAl coating used for comparison purpose was sprayed under the following conditions: standoff distance of 200 mm, voltage of 32 V, current of 160 A, and pressure of 0.6 MPa [18]. The voltage and current spraying parameters of the composite coating were varied accordingly, as shown in Table 2, in order to achieve a stable arc and optimize the properties of the coating. The standoff distance for the composite coating was 200 mm. FeCrAl/Al composite coatings with varying parameters are referred to as #A, #B, #C, and #D.

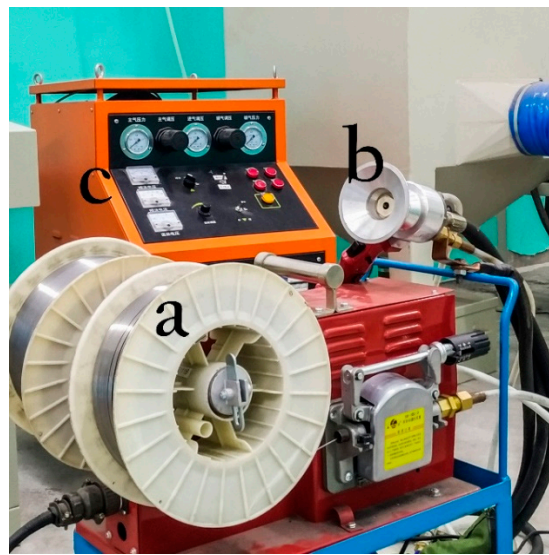


**Figure 1.** LSARC arc spraying equipment: (a) Wire feed, (b) spray gun, and (c) spray controller and power supply.

**Table 2.** Process parameters.

Sample	Voltage (V)	Current (A)
#A	32	160
#B	36	200
#C	40	220
#D	44	260
FeCrAl	32	160

### 2.3. Surface Morphology Evaluation

The surface characterization and cross-sectional microstructure of the HVAS coatings and the corroded coatings were examined by a FEI Quanta FEG 250 scanning electron microscope (SEM, Thermo Fisher Scientific, Waltham, MA, USA). Phase composition of the coatings was analyzed using X'Pert powder X-ray diffraction (XRD, Malvern Panalytical, Malvern, Worcestershire, UK) apparatus with Cu K $\alpha$  radiation ( $\lambda = 1.5406$  nm) generated at 40 kV and 40 mA. Image analysis software ImageJ (ImageJ 1.52a) was employed to measure the average porosity of the coatings. The procedure was listed as follows: the cross-sectional images were collected and input in the software; images were processed and porosity recorded [13]. An average value of porosity was taken from 15 cross-section images for each sample.

Scratch adhesion strength of the coatings to substrate was measured with CETR-Universal Materials Tester (CETR-UMT, Bruker, Billerica, MA, USA) according to ASTM C1624-05 standard [21]. A constant normal load of 150 N was applied to the sample coatings. The scratch length was 7 mm and loading rate of 100 N/min. The average adhesion strength was calculated from five measurements [22].

### 2.4. Microhardness Test

The coating hardness was measured by the Automatic Tester Duramin-40 machine (Ballerup, Copenhagen, Denmark) with a pyramidal indenter. The applied load and dwelling time for the hardness test were 100 gf and 15 s respectively. Vickers microhardness test was measured along the plane of the cross section of coatings. Hardness value was calculated from 15 measurements of each

polished sample to ensure repeatability. The indentation diameter is converted into microhardness units (HV) using the applied Equation (1), as shown below [23].

$$HV = \frac{1.8544 \times F}{d^2} \quad (1)$$

where HV is the Vickers hardness,  $F$  is the force applied, and  $d$  is the average of two diagonals.

### 2.5. Corrosion Test

Corrosion of the samples was quantified via a potentiodynamic polarization technique employing a three-electrode configuration, consisting of the saturated calomel electrode (SCE) as reference, platinum as counter electrode, and the coated samples as working electrode. The corrosion resistance was tested by electrochemical work station (CS350, Wuhan Corrtest Instruments Corp., Ltd., Wuhan, China). The samples were connected to electrical wires in order to allow electrochemical measurements and embedded in an epoxy resin to seal off surface pores. The coated area of 1 cm<sup>2</sup> was left exposed to the 3.5 wt.% sodium chloride (NaCl) electrolyte at room temperature (25 °C, pH 6.5). Potentiodynamic polarization was measured at the scan rate of 0.5 mV/s and frequency range of the electrochemical impedance spectroscopy test (EIS) was from 100 kHz to 10 mHz. The polarization resistance was calculated by the Stern–Geary relationship [24]. The polarization resistance,  $R_p$ , of a material is defined as the slope of the potential–current density ( $dE/di$ ) curve at the free corrosion potential, yielding the polarization resistance as shown in Equation (2):

$$R_p = \frac{\beta_a \beta_c}{2.3(\beta_a + \beta_c)} \times \frac{1}{i_{\text{corr}}} = \frac{\Delta E}{\Delta i} \quad (2)$$

where  $i_{\text{corr}}$  is the current density.

The proportionality constant  $B$  [25], can be empirically obtained from  $\beta_a$  and  $\beta_c$  the slopes of the anodic and cathodic Tafel, respectively, as shown in Equation (3):

$$B = \frac{\beta_a \beta_c}{2.3(\beta_a + \beta_c)} \quad (3)$$

After the coatings were exposed for 1 h in the NaCl solution, the corrosion rate of the coatings in mm/yr was derived from the Faraday's law [26,27] using Equation (4):

$$\text{Corrosion rate} \left( \frac{\text{mm}}{\text{yr}} \right) = \frac{3272 i_{\text{corr}} EW}{dA} \quad (4)$$

where  $i_{\text{corr}}$  is the corrosion current density in  $\mu\text{A}/\text{cm}^2$ ,  $EW$  is the Equivalent weight in grams,  $d$  is the density in  $\text{g}/\text{cm}^3$ , and  $A$  is the area of the sample in  $\text{cm}^2$ .

## 3. Results and Discussions

### 3.1. Microstructure of the Coating

Figure 2 illustrates the surface morphology of the coatings. The surface images show disk-shaped individual splat droplets and flattened areas formed by high velocity impact of molten droplets on the substrate. Coatings #C and #D display more flattened areas, showing a better spreadability of the molten material with little splashing. It is commonly depicted that thermal spray particles have good spreadability and high degree of deformation in the more flattened areas [28]. Increasing the voltage lead to increase in arc temperature, and hence there is more energy to heat the particles; however, the spray velocity decreases [29]. This affects bonding enhancement of coating to the substrate material. Increase in the voltage from 32 to 44 V raised the arc temperature which resulted in splats forming circular disks, and increase in the arc voltage decreased diameter of the droplets formed at the wire

tip [12]. Coatings #A and #B were of lower voltage, and thus the droplets splashed on the surface forming irregular splats. Low voltage and current could not provide sufficient heat energy to melt all the particles, thus resulted in nonuniform microstructure of the coatings. On the other hand, higher current supplies more heat input to the molten droplets which helps to improve interaction between the droplets and the substrate at the interface [30]. The particles were completely melted to produce flattened splats.

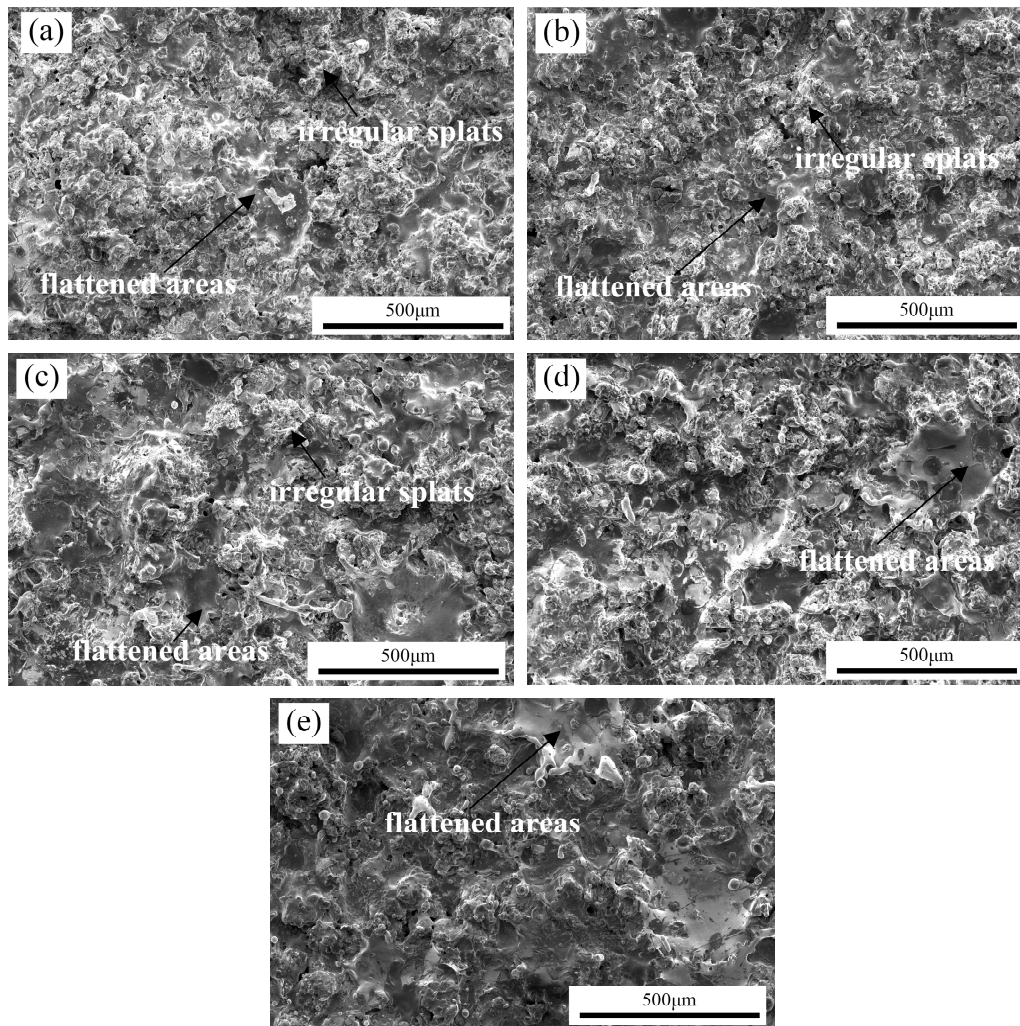


**Figure 2.** Surface morphology images of the coatings: (a) #A, (b) #B, (c) #C, (d) #D and (e) FeCrAl.

The average porosities of the coatings are listed in Table 3. FeCrAl coating, #A, #B, #C, and #D had porosities of 3.77, 5.34, 4.97, 4.29, and 3.46 (%), respectively. Coating #D had the lowest porosity, which implies a denser compact structure than FeCrAl coating.

**Table 3.** Properties of the coatings.

Coating	Microhardness, HV <sub>0.1</sub>	Scratch-Test Adhesion Strength (N)	Porosity, %	Surface Roughness, R <sub>a</sub> (µm)
FeCrAl	409.10	40.12 ± 2.11	3.77 ± 0.82	1.63 ± 0.39
#A	329.10	41.02 ± 7.41	5.34 ± 1.13	1.79 ± 0.36
#B	332.80	45.10 ± 10.65	4.97 ± 1.29	2.27 ± 0.13
#C	394.33	48.17 ± 8.96	4.29 ± 1.39	2.44 ± 0.07
#D	513.51	67.43 ± 13.02	3.46 ± 0.84	2.93 ± 0.33

Cross-sectional SEM images of both the composite coating FeCrAl/Al and FeCrAl are shown in Figure 3, the average coating thickness was  $335 \pm 4 \mu\text{m}$ . The cross-section images show typical lamellar structure characterized by Fe-based metallic phases, Al splats, semi-melted particles, oxide layers, and some pores. The composite coating displays relatively long alternating layers of FeCr and Al uniformly distributed on the substrate surface, indicating good wettability and spreadability of the particles. The molten droplets distributed evenly on the substrate surface to form layers that stacked on top of each other to form the coating [13,31]. Al particles were homogeneously distributed throughout the microstructure of the coating.

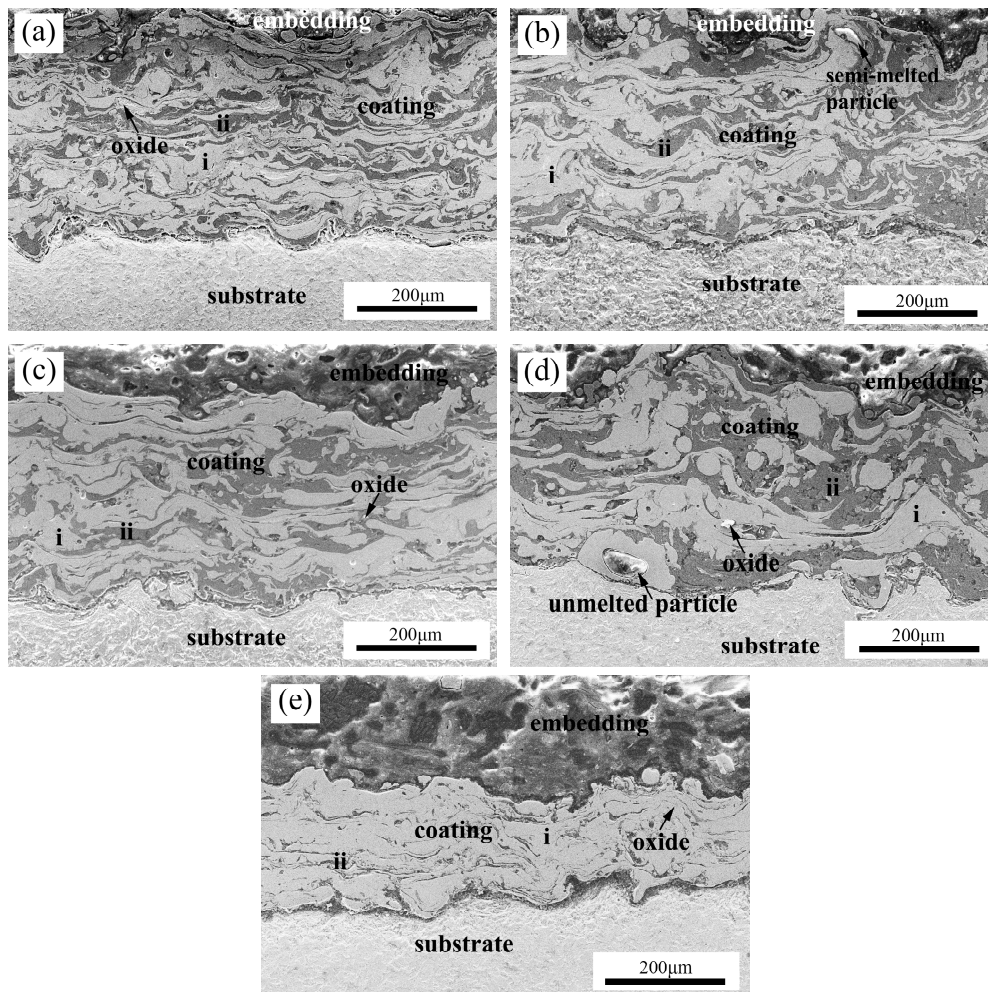


**Figure 3.** Cross-section images of the coatings (a) #A, (b) #B, (c) #C, (d) #D and I FeCrAl with (i) matrix phase comprised of FeCr, AlFe,  $\text{Cr}_2\text{O}_3$ , and (ii) aluminum and aluminum oxides.

It is also evident from the cross-sectional images that splats of FeCrAl/Al coating were thicker than those of the FeCrAl coating. From a combination of the cross-sectional images, XRD, and EDS results, the light gray region (i) in Figure 3 is the matrix phase comprised of iron–chromium (FeCr), AlFe intermetallic compound and chromium oxide ( $\text{Cr}_2\text{O}_3$ ); The dark gray region (ii) comprises of aluminum and aluminum oxides ( $\text{Al}_2\text{O}_3$ ).

The EDS analysis on Figure 4 shows an increase in the amount of Aluminum content in the composite coatings. The chemical compositions of FeCrAl and FeCrAl/Al coatings were  $\text{Fe}_{74.94}$ ,  $\text{Cr}_{16.82}$ , and  $\text{Al}_{8.24}$ , and  $\text{Fe}_{37.81}$ ,  $\text{Cr}_{6.06}$ , and  $\text{Al}_{56.13}$  (at.%), respectively.

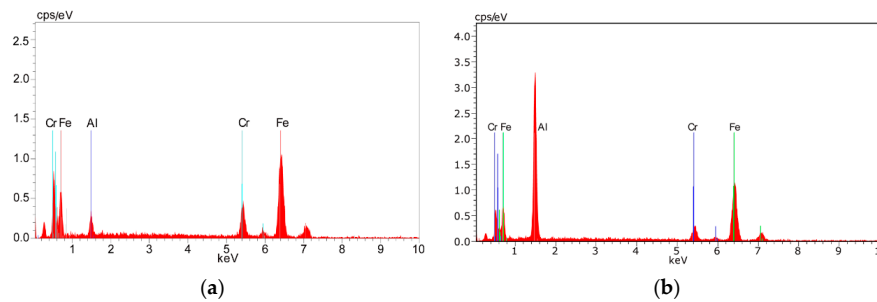


**Figure 4.** Energy-dispersive X-ray spectroscopy (EDS) analysis of the (a) FeCrAl coating and (b) FeCrAl/Al coating.

### 3.2. XRD Patterns

Figure 5 shows the XRD patterns of different FeCrAl/Al composite coatings. The diffraction peaks that correspond to FeCr, Al, AlFe intermetallic compound,  $\text{Cr}_2\text{O}_3$ , and  $\text{Al}_2\text{O}_3$  were observed. FeCr and Al were the principle phases of the composite coatings. The oxide phases detected ( $\text{Cr}_2\text{O}_3$  and  $\text{Al}_2\text{O}_3$ ) were formed during the spraying process when the inflight molten particles interact with the atmospheric oxygen and when the molten particles hit the substrate. Oxides had an effect on corrosion resistance of the coatings and reduced the porosity of the coatings [32]. During spraying of FeCrAl/Al composite coating, the amount of Al increased with the increasing voltage from 32 to 44 V and the highest peak of Al formed in #D coating. The Al peak for the #B coating was nearly as high as that of the #D coating. This anomaly could be as a result of the arc instability between the two wire feeds. As compared to the FeCrAl coating, the FeCr phase was observed to be lower in the composite coatings. The amount of the Al phase as supported by the EDS results, increased with increase in voltage and current, however inhibiting formation of the FeCr phase in the composite coatings. The higher amount of Al could be attributed to the increase in voltage that raised the amount of heat required to melt the feed material [14,31]. Due to the lower melting point of Al, a higher amount of Al was introduced into the molten arc thus the higher Al peak. The melting extent of coating particles and the amount of decomposed phases were enhanced with increasing spraying power [15].

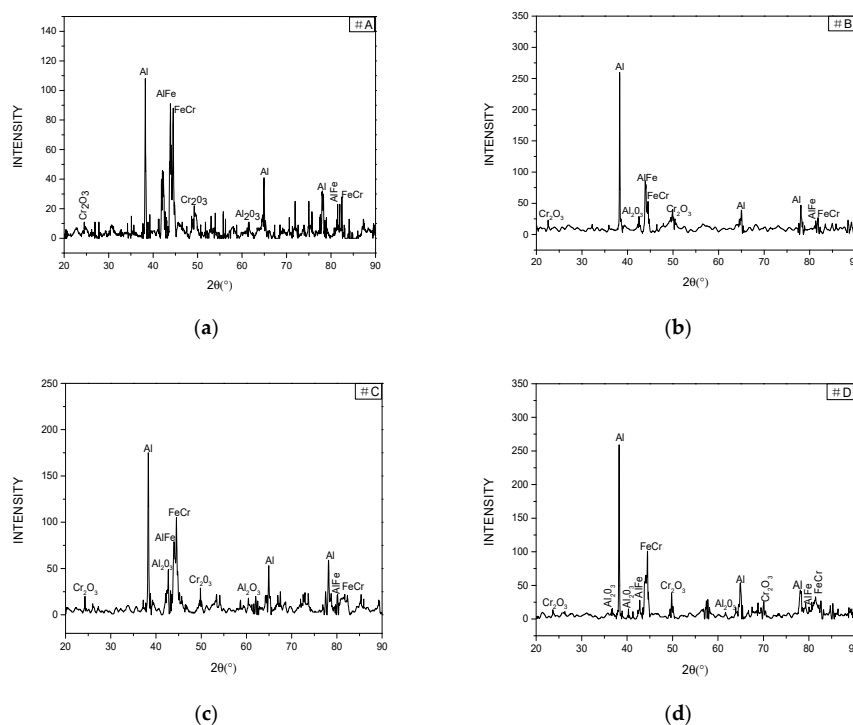


**Figure 5.** Cont.

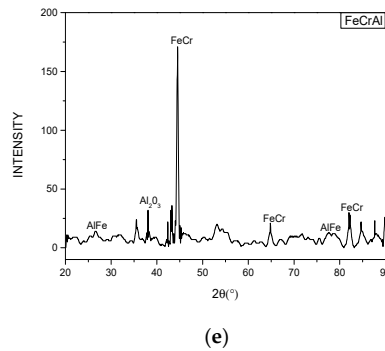


**Figure 5.** XRD patterns of the coatings (a) #A, (b) #B, (c) #C, (d) #D, and (e) FeCrAl.

The AlFe phase alloys that were detected in the XRD analysis explain the possibility of an intermetallic reaction between FeCrAl and aluminum during the spraying process. These phase alloys were formed on a diffusion layer which was found at the FeCrAl and Al substrate interface as a result of mixing of FeCrAl and Al during the spraying process [33]. Al has a lower melting point of approximately 660 °C, whereas FeCrAl alloy has a higher melting point of approximately 1500 °C, and therefore Al readily melted and reacted with the Fe rich alloy forming FeAl. The composite coating was, therefore, an interwoven mixture between FeCrAl and Al to form interlamellar structure with aluminium splats and FeCrAl splats [13,34].

### 3.3. Microhardness

Properties of the coatings are listed in Table 3. Figure 6 shows the microhardness of both the coatings and substrate. The average hardness of the mild steel substrate was 165.52 HV<sub>0.1</sub>, while that of the composite coatings ranged between 329.10 and 513.51 HV<sub>0.1</sub>, which is related to the varying voltage and current. The hardness of the composite coating #D is ~2–3 times in comparison with the substrate. In addition, microhardness of the composite coating #D was higher than that of the FeCrAl coating as shown in Figure 6. The increase in voltage decreased the size of molten particles. Larger surface area of the smaller droplets made them more prone to be oxidized during the inflight and to the point of deposition. Oxidation of these molten droplets during spraying process was likely to increase coating hardness [6,35]. The presence of increased Al and the Cr in the alloy wire form films of protective oxides Al<sub>2</sub>O<sub>3</sub> and Cr<sub>2</sub>O<sub>3</sub> respectively, contributing to the high hardness of the composite coating #D [36]. High current and voltage increase the ability of the molten particles to bond with the substrate and the coating was characterized with fewer microcracks on the surface, hence significant increase in the microhardness. This can be explained that the surface structure of coatings #C and #D displayed good spreadability of the molten particles and possessed a more compact structure with fewer pores. Coatings #A and #B had less of a compact structure with some unmelted particles that affected the microhardness of the coating. However, the increase in Aluminum content had a significant effect on the overall microhardness of the coating because microhardness was low in areas where there were layers of Al. The FeCrAl/Al composite coating formed interwoven layers of hard and ductile phases which is consistent with a former study [11]. As the voltage of the coatings increased, the particle velocity reduced. As reported, as arc current increases the surface roughness slightly increases the wire feed rate. The higher wire feed rate increased in the amount of material atomized resulting in less efficient atomization and larger particles [37]. The surface roughness increased as listed in Table 3. The highest surface roughness was achieved on coating #D which had the highest current.

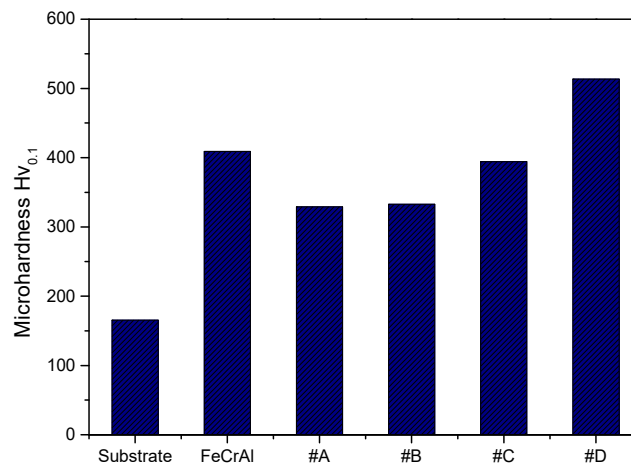


**Figure 6.** Vickers microhardness of high velocity arc spraying (HVAS) coatings.

The adhesion strength of particles, as shown in Table 3, improved relatively with increase in the operating voltage and current [12]. The adhesion strength shows the combinative characteristics of the coating and substrate. The adhesion strength of FeCrAl coating was 40.12 N, which was lower than the FeCrAl/Al composite coatings. Coating #D had the highest adhesion strength of 67.43 N. Different parameters such as the porosity and oxides affect the adhesion strength [28]. Adhesion strength of the #D coating was highest due to its good wettability and spreadability of the molten droplets. The adhesion strength of the coatings followed a similar trend as the microhardness.

#### 3.4. Corrosion Behavior

Figure 7 illustrates the potentiodynamic polarization curves of the coatings. The corrosion current densities and corrosion potentials extrapolated from the Tafel curves are presented in Table 4. The polarization resistance  $R_p$  as shown in Table 4 was obtained using the Stern–Geary equation. According to the results obtained, it is noted that FeCrAl coating has a current density of  $14.95 \mu\text{A}/\text{cm}^2$  while Coating #D has a current density of  $7.44 \mu\text{A}/\text{cm}^2$ , which is less than the former. Current density is the main parameter used to measure the efficiency of protective coating kinetics; the higher the current density, the poorer the electrochemical behavior. This indicates that the coating #D passivates more than the other composite coatings due to its lowest current density.

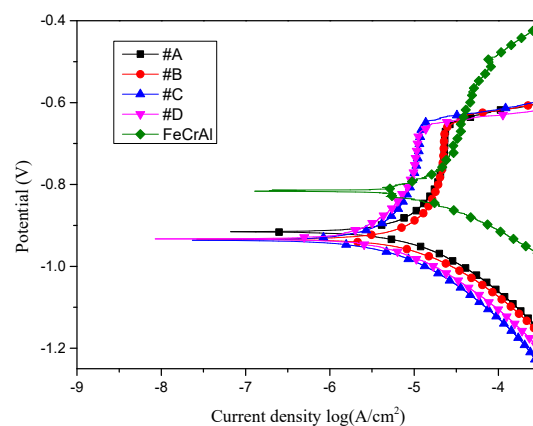


**Figure 7.** Potentiodynamic polarization curves of the composite coatings and FeCrAl coating.

**Table 4.** Potentiodynamic polarization parameters of the sprayed coatings.

Coatings	$\beta_a$ (mV)	$\beta_c$ (mV)	$i_{corr}$ ( $\mu\text{A}/\text{cm}^2$ )	$E_{corr}$ (V)	Corrosion Rate (mm/yr)	$R_p$ ( $\text{k}\Omega/\text{cm}^2$ )
FeCrAl	343.05	114.72	14.95	−0.82	0.18	2500.00
#A	1237.80	181.93	18.35	−0.92	0.22	3758.04
#B	8182.80	194.44	23.38	−0.93	0.28	3531.34
#C	1138.60	157.92	7.69	−0.94	0.09	7841.06
#D	2263	139.77	7.44	−0.93	0.09	7690.75

This difference can be attributed to the increased amount of Aluminum in the composite coatings. Al corrosion resistance is dependent upon protective oxide films that inhibit the electrolyte penetration into the substrate. The stable  $\text{Al}_2\text{O}_3$  oxide layer, as shown in XRD, acts as a physical barrier against the corrosive environment. The passivating layer of  $\text{Cr}_2\text{O}_3$  also enhances the corrosion resistance of the coating. As for the composite coatings there was no significant change in the corrosion potential ( $E_{corr}$ ). It is noted that coating #C had a more negative corrosion potential.

Coating #A has corrosion potential of  $-0.92$  V and current density of  $18.35 \mu\text{A}/\text{cm}^2$ . The coating exhibited low corrosion resistance because of its structural imperfection that was exposed to the electrolyte. The pores and cracks in the coating caused by high porosity act as the channels for the  $\text{Cl}^-$  ions to penetrate into the coating [38,39]. The presence of defects and pores in the coating allow electrolyte diffusion, thus promoting the failure of the protective coating.

The data in the Table 4 shows that current density of the composite coatings first increased and then decreased with increase in the voltage and current.

The highest polarization resistances were detected in coatings #C and #D, which are approximately three times that of the FeCrAl coating. Thus, effect of simultaneous spraying with Al and increasing the voltage and current of the coating resulted in the better corrosion resistance. In addition, the lamellar structure of the coating improved corrosion resistance because of reduced pores and cracks that would cause pitting. [40]. The smooth flattened splats in the coatings #C and #D contributed to a compact structure with few pores and cracks, slowing the penetration of NaCl solution.

Coating #D had the lowest corrosion rate and current density which indicates that the voltage had an effect on the corrosion resistance. From the XRD results, Al content increased with the increase in voltage and thus improved corrosion properties of the composite coating. This can also be attributed to the dense structure of the coating, with reduced porosity, formed by the molten particles on impact [3,41]. From the observations, it is noted that the coatings #C and #D had better corrosion properties. Simultaneous arc spraying of FeCrAl and Al and increasing the voltage and current improved the corrosion properties of the traditional FeCrAl coating.

The surface of the coatings was mostly covered by the corrosion products of the composite coatings as shown in Figure 8. The white layer on the surface likely suggests the passivation films formed after oxidation of Al and Cr to form thin oxide films that prevent further penetration of the solution. These corrosion products therefore enhanced protective barrier for the coatings.

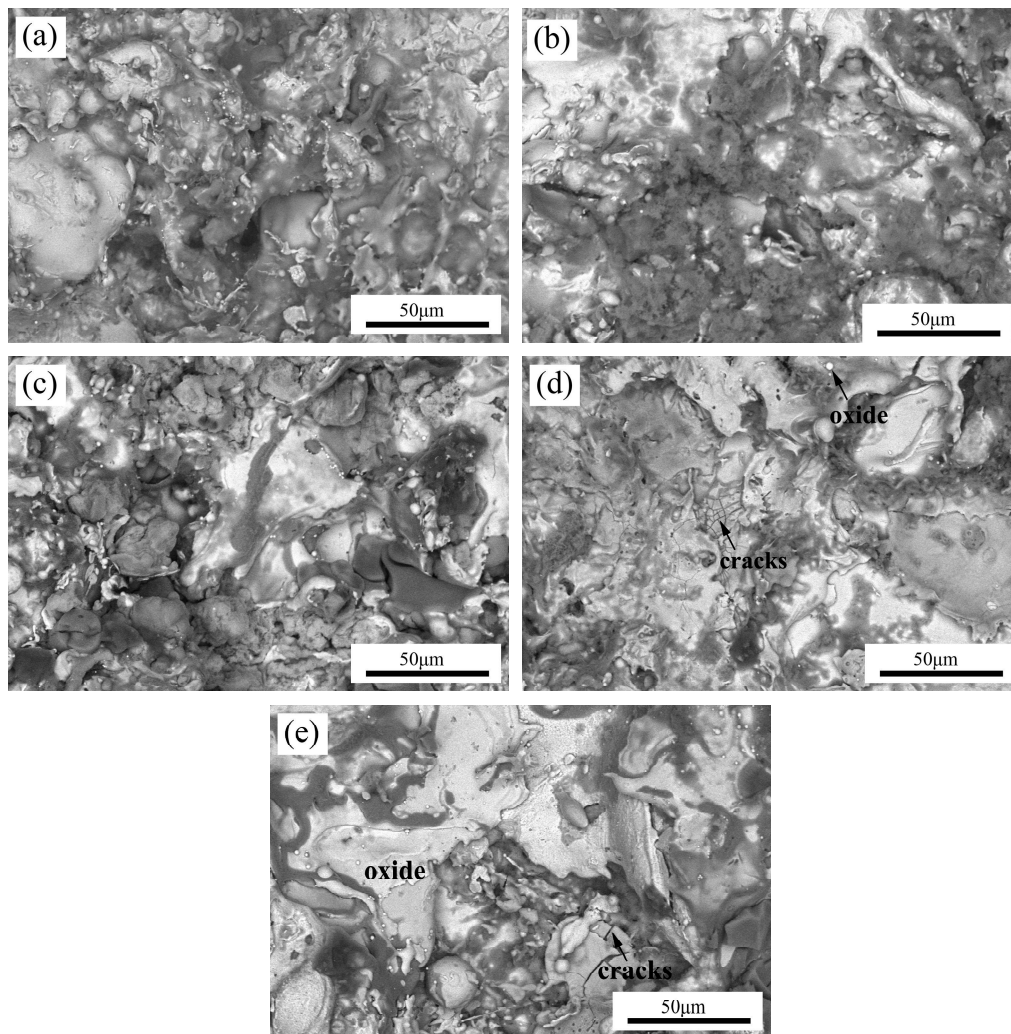


**Figure 8.** Surface morphologies of the coatings after corrosion (a) #A, (b) #B, (c) #C, (d) #D, and (e) FeCrAl.

#### 4. Conclusions

- A composite material, FeCrAl/Al, was successfully prepared by high velocity arc spraying two different metal wires using FeCrAl as the anode and aluminum as the cathode. The voltage and current of spraying materials were varied to achieve the optimum spraying parameters for the coatings.
- Microstructure of the coatings were quite similar exhibiting a typical lamellar type structure with alternating layers of FeCrAl and Al. Increasing voltage and current resulted in smooth flattened areas, hence improved the spreadability of the molten particles. FeCrAl/Al coatings were composed of Al and FeCr as the main phases with presence of intermetallic compounds AlFe.
- The increase in voltage and current improved the mechanical properties of the coatings as well. The microhardness increased and was highest in coating #D (513.15 HV<sub>0.1</sub>) with alternating layers of hard and ductile phases. Good spreadability and deformation of the molten particles at higher voltage improved the adhesion strength of coating to the substrate hence, reduced average porosity and increased microhardness of the composite coating. The average adhesion strength of the composite coating increased from 41.02 to 67.43 N. The results indicate that 44 V and 260 A was the best combination under the tested conditions, in which the Q235 substrate bonds well with the FeCrAl/Al coating, enhancing the adhesion strength.

- Results of the polarization test showed that the composite coatings with higher voltage and current contributed to good corrosion resistance. The composite coating had better corrosion resistance than the traditional FeCrAl coating. The FeCrAl/Al composite can therefore be used to protect steel structures from NaCl aqueous solutions.

**Author Contributions:** Conceptualization, N.J.N. and M.K.; Methodology, N.J.N., S.M.N., Y.L., and F.H.; Software, N.J.N. and Y.L.; Validation, J.L. and N.J.N.; Formal Analysis, N.J.N.; Investigation, N.J.N. and M.K.; Resources, M.K.; Data Curation, N.J.N. and Y.L.; Writing—Original Draft Preparation, N.J.N. and S.M.N.; Writing—Review and Editing, N.J.N., M.K., and J.L.; Visualization, N.J.N.; Supervision, M.K.; Project Administration, M.K.; J.Z.; Funding Acquisition, M.K.

**Funding:** The research was funded by the Technology development programmer for the Northern Jiangsu area, (Grant No. BN2014019).

**Acknowledgments:** The authors gratefully acknowledge the support of the Research Institute of Nanjing Chemical Industry Group, Sinopec.

**Conflicts of Interest:** The authors declare no conflict of interest.

## References

1. Qiang, L.A.; Kui, X.; Fang, D.C.; Gang, L.X. Corrosion behaviour of Zn-Al pseudo-alloy coating on carbon steel in chloride environments. In *Advanced Materials Research*; Trans Tech Publications: Stafa-Zurich, Switzerland, 2012; Volume 567.
2. Esfahani, E.A.; Salimijazi, H.; Golozar, M.A.; Mostaghimi, J.; Pershin, L. Study of corrosion behavior of arc sprayed aluminum coating on mild steel. *J. Therm. Spray Technol.* **2012**, *21*, 1195–1202. [[CrossRef](#)]
3. Cheng, J.; Wang, Z.; Xu, B. Wear and corrosion behaviors of FeCrBSiNbW amorphous/nanocrystalline coating prepared by arc spraying process. *J. Therm. Spray Technol.* **2012**, *21*, 1025–1031. [[CrossRef](#)]
4. Pawlowski, L. *The Science and Engineering of Thermal Spray Coatings*; John Wiley & Sons: Hoboken, NJ, USA, 2008.
5. Chen, T.-C.; Chou, C.-C.; Yung, T.-Y.; Tsai, K.-C.; Huang, J.-Y. Wear behavior of thermally sprayed Zn/15Al, Al and Inconel 625 coatings on carbon steel. *Surf. Coat. Technol.* **2016**, *303*, 78–85. [[CrossRef](#)]
6. Gedzevicius, I.; Valiulis, A. Analysis of wire arc spraying process variables on coatings properties. *J. Mater. Process. Technol.* **2006**, *175*, 206–211. [[CrossRef](#)]
7. Brezinová, J.; Landová, M.; Guzanová, A.; Dulebová, L.; Draganovská, D. Microstructure, Wear Behavior and Corrosion Resistance of WC-FeCrAl and WC-WB-Co Coatings. *Metals* **2018**, *8*, 399. [[CrossRef](#)]
8. Gorlach, I. A new method for thermal spraying of Zn–Al coatings. *Thin Solid Film.* **2009**, *517*, 5270–5273. [[CrossRef](#)]
9. Bratean, L. Thermal spraying arc process with two dissimilar wires—quality tests. *Procedia Soc. Behav. Sci.* **2015**, *180*, 1116–1121. [[CrossRef](#)]
10. Watanabe, T.; Sato, T.; Nezu, A. Electrode phenomena investigation of wire arc spraying for preparation of Ti-Al intermetallic compounds. *Thin Solid Film.* **2002**, *407*, 98–103. [[CrossRef](#)]
11. Chen, Y.-X.; Xu, B.-S.; Yan, L.; Liang, X.-B.; Yi, X. Structure and sliding wear behavior of 321 stainless steel/Al composite coating deposited by high velocity arc spraying technique. *Trans. Nonferr. Met. Soc. China* **2008**, *18*, 603–609. [[CrossRef](#)]
12. Wang, Z.J.; Zhu, G.M.; Yin, F.S. Study on the microstructure of FeCrAl/aluminum bronze composite coatings prepared by supersonic electric arc-spraying. In *Applied Mechanics and Materials*; Trans Tech Publications: Stafa-Zurich, Switzerland, 2012; pp. 1346–1349.
13. Tian, H.; Wang, C.; Guo, M.; Tang, Z.; Wei, S.; Xu, B. Phase composition and formation mechanisms of a high-velocity electric arc-sprayed FeNiCrAl coating. *J. Alloys Compd.* **2018**, *769*, 998–1006. [[CrossRef](#)]
14. Newbery, A.; Grant, P. Oxidation during electric arc spray forming of steel. *J. Mater. Process. Technol.* **2006**, *178*, 259–269. [[CrossRef](#)]
15. Wang, R.; Song, D.; Liu, W.; He, X. Effect of arc spraying power on the microstructure and mechanical properties of Zn–Al coating deposited onto carbon fiber reinforced epoxy composites. *Appl. Surf. Sci.* **2010**, *257*, 203–209. [[CrossRef](#)]

16. Cebulski, J.; Pasek, D. FeAl intermetallic alloy: Its heat-resistant and practical application. In *Intermetallic Compounds: Formation and Applications*; Aliofkhaezrai, M., Ed.; Books on Demand: Norderstedt, Germany, 2018; Chapter 1.
17. Xu, W.-P.; Xu, B.-S.; Zhang, W.; Wu, Y.-X. Erosion-corrosion behaviors of High Velocity Arc Sprayed Fe-Al/Cr<sub>3</sub>C<sub>2</sub> Coating. *J. Wuhan Univ. Technol. Mater. Sci. Ed.* **2006**, *21*, 29–31.
18. Liu, G.; Roźniatowski, K.; Kurzydłowski, K. Quantitative characteristics of FeCrAl films deposited by arc and high-velocity arc spraying. *Mater. Charact.* **2001**, *46*, 99–104. [[CrossRef](#)]
19. Lei, Y.; Qiu, Z.; Liu, J.; Li, D.; Tan, N.; Liu, T.; Zhang, Y.; Chang, X.; Gu, Y.; Yin, Y. Effect of Conducting Polyaniline/Graphene Nanosheet Content on the Corrosion Behavior of Zinc-Rich Epoxy Primers in 3.5% NaCl Solution. *Polymers* **2019**, *11*, 850. [[CrossRef](#)] [[PubMed](#)]
20. Gharahcheshmeh, M.H.; Sohi, M.H. Study of the corrosion behavior of zinc and Zn–Co alloy electrodeposits obtained from alkaline bath using direct current. *Mater. Chem. Phys.* **2009**, *117*, 414–421. [[CrossRef](#)]
21. *ASTM C162-05 Standard Test Method for Adhesion Strength and Mechanical Failure Modes of Ceramic Coatings by Quantitative Single Point Scratch Testing*; ASTM International: West Conshohocken, PA, USA, 2005.
22. Gonczy, S.T.; Randall, N. An ASTM standard for quantitative scratch adhesion testing of thin, hard ceramic coatings. *Int. J. Appl. Ceram. Technol.* **2005**, *2*, 422–428. [[CrossRef](#)]
23. Szymanski, A.; Szymanski, J.M. *Hardness estimation of minerals, rocks and ceramic materials*; Elsevier: Amsterdam, The Netherlands, 1989.
24. Ahmad, Z. *Principles of Corrosion Engineering and Corrosion Control*; Elsevier: Amsterdam, The Netherlands, 2006.
25. Revie, R.W. *Corrosion and Corrosion Control: An Introduction to Corrosion Science and Engineering*; John Wiley & Sons: Hoboken, NJ, USA, 2008.
26. Choe, H.-B.; Lee, H.-S.; Shin, J.-H. Experimental study on the electrochemical anti-corrosion properties of steel structures applying the arc thermal metal spraying method. *Materials* **2014**, *7*, 7722–7736. [[CrossRef](#)]
27. Dean, S.W. *Corrosion Testing of Materials with Metallic and Inorganic Coatings*. In *Testing of Metallic and Inorganic Coatings*; ASTM International: West Conshohocken, PA, USA, 1987.
28. Zhang, X.; Wang, Z.; Lin, J.; Zhou, Z. A study on high temperature oxidation behavior of high-velocity arc sprayed Fe-based coatings. *Surf. Coat. Technol.* **2015**, *283*, 255–261. [[CrossRef](#)]
29. Newbery, A.; Grant, P.; Neiser, R. The velocity and temperature of steel droplets during electric arc spraying. *Surf. Coat. Technol.* **2005**, *195*, 91–101. [[CrossRef](#)]
30. Harju, A. Properties of high velocity arc sprayed coatings. Master's Thesis, Tampere University of Technology, Tampere, Finland, 2017.
31. Abkenar, A.P. Wire-arc Spraying System: Particle Production, Transport, and Deposition. Ph.D. Thesis, University of Toronto, Toronto, ON, Canada, 2007.
32. Luo, L.-M.; Liu, S.-G.; Jia, Y.; Juan, L.; Jian, L. Effect of Al content on high temperature erosion properties of arc-sprayed FeMnCrAl/Cr<sub>3</sub>C<sub>2</sub> coatings. *Trans. Nonferr. Met. Soc. China* **2010**, *20*, 201–206. [[CrossRef](#)]
33. Li, Q.; Song, P.; Ji, Q.; Huang, Y.; Li, D.; Zhai, R.; Zheng, B.; Lu, J. Microstructure and wear performance of arc-sprayed Al/316L stainless-steel composite coating. *Surf. Coat. Technol.* **2019**, *374*, 189–200. [[CrossRef](#)]
34. Tian, H.; Wei, S.; Chen, Y.; Tong, H.; Liu, Y.; Xu, B. Wear behavior of high velocity arc spraying FeNiCrAlBRE/Ni95Al composite coatings. *Phys. Procedia* **2013**, *50*, 282–287. [[CrossRef](#)]
35. Gedzevičius, I.; Valiulis, A. Influence of the particles velocity on the arc spraying coating adhesion. *Matrix* **2003**, *1*, 3.
36. Chao, Y.J.; Weng, J.J.; Liu, S.G.; Li, J.; Sang, J.P. The Structures and High Temperature Properties of FeMnCrNiAl/Cr<sub>3</sub>C<sub>2</sub> Composite Coatings by High Velocity Arc Spraying. In *Applied Mechanics and Materials*; Trans Tech Publications: Stafa-Zurich, Switzerland, 2012; pp. 1532–1538.
37. Johnston, A.L.; Hall, A.C.; McCloskey, J.F. Effect of process inputs on coating properties in the twin-wire arc zinc process. *J. Therm. Spray Technol.* **2013**, *22*, 856–863. [[CrossRef](#)]
38. Li, H.; Duan, J.; Wei, D. Comparison on corrosion behaviour of arc sprayed and zinc-rich coatings. *Surf. Coat. Technol.* **2013**, *235*, 259–266. [[CrossRef](#)]
39. Li, H.; Wei, D.; Duan, J.; Zhou, J.; Min, X. Effect of sealing treatment on corrosion behaviours of arc sprayed zinc coatings. *Corros. Eng. Sci. Technol.* **2013**, *48*, 65–70. [[CrossRef](#)]

40. Lin, J.; Wang, Z.; Lin, P.; Cheng, J.; Zhang, J.; Zhang, X. Microstructure and corrosion resistance of Fe-based coatings prepared by twin wires arc spraying process. *J. Therm. Spray Technol.* **2014**, *23*, 333–339. [[CrossRef](#)]
41. Tang, J.; Zhu, Q.; Wang, Y.; Apreutesei, M.; Wang, H.; Steyer, P.; Chamas, M.; Billard, A. Insights on the Role of Copper Addition in the Corrosion and Mechanical Properties of Binary Zr-Cu Metallic Glass Coatings. *Coatings* **2017**, *7*, 223. [[CrossRef](#)]



© 2019 by the authors. Licensee MDPI, Basel, Switzerland. This article is an open access article distributed under the terms and conditions of the Creative Commons Attribution (CC BY) license (<http://creativecommons.org/licenses/by/4.0/>).